Multifunctional Nanobeads Based on Quantum Dots and Magnetic Nanoparticles: Synthesis and Cancer Cell Targeting and Sorting

Riccardo Di Corato,[†,‡] Nadja C. Bigall,[‡] Andrea Ragusa,[†,‡] Dirk Dorfs,[‡] Alessandro Genovese,[‡] Roberto Marotta,[‡] Liberato Manna,[‡] and Teresa Pellegrino*[,†,‡]

[†]Nanoscience Institute of CNR, National Nanotechnology Laboratory, Via Arnesano 16, 73100 Lecce, Italy, and [‡]Italian Institute of Technology (IIT), Via Morego 30, 16163 Genova, Italy

ABSTRACT Trifunctional polymer nanobeads are prepared by destabilization of a mixture of magnetic nanoparticles, quantum dots, and an amphiphilic polymer, followed by functionalization of the bead surface with folic acid molecules. The distribution of the nanoparticles within the nanobeads can be tuned using either acetonitrile or water as destabilizing solvent. The luminescence of the resulting beads can be tuned by varying the ratio of quantum dots per magnetic nanoparticles. The application of an external magnetic field (such as a small static magnet of 0.3 T) to the magnetic–fluorescent nanobeads allows the quantitative accumulation of the beads within a few hours depending on the total size of the beads. Furthermore, specific targeting of cancer cells overexpressing folate receptors is achieved thanks to the folic acid decorating the surface of the as-synthesized nanobeads. Folate receptor mediated cellular uptake of the folic acid-functionalized nanobeads is proven *via* both confocal imaging and transmission electron microscopy characterization. Cell sorting experiments performed with trifunctional nanobeads show quantitative recovering of targeted cells even when they are present at low percentage (up to 1%).

KEYWORDS: magnetic nanoparticles · quantum dots · magnetic–fluorescent nanostructures · magnetic clusters · cell sorting · tumor labeling

Recently, there has been remarkable progress in the synthesis of colloidal nanoparticles and in their exploitation for various applications.[1−3] Examples are monodisperse superparamagnetic nanoparticles, which are finding applications in magnetic resonance imaging, magnetically guided drug delivery, hyperthermia and cell separation,[4−8] and semiconductor core–shell nanostructures, also known as quantum dots (QDs) with tunable optical properties and high fluorescence quantum yield,[9,10] for applications in biological and medical imaging.[11−14] In addition, a new trend in material science has emerged in the last years, which focuses on the development of multifunctional nanostructures by packing together the attractive properties of both magnetic and fluorescent nanoparticles into single nanoobjects, which are often made of polymeric (nano)beads.[15−22] In this regard, when the targeted application is bioseparation and detection, the system should be properly designed in order to meet a large set of challenges.[23−27]

Inorganic superparamagnetic nanoparticles offer the potential advantage of exhibiting an induced magnetic moment whenever an external magnet is positioned close to them, while they do not retain any residual magnetization upon removal of the external field, and thus in the absence of the magnet they do not aggregate.[28] While this is a desirable property in biomedical applications, the magnetization associated with each individual nanoparticle is quite small, and therefore the nanoparticles do not accumulate on the magnet within a reasonable time frame, which is a clear limitation for applications involving magnetic separation of cells. Controlled clustering of multiple superparamagnetic nanoparticles into nanoscale superstructures, as in the case of polymeric nanobeads, has on the other hand the advantage to retain the superparamagnetic behavior of the individual nanoparticles, while resulting in a faster accumulation on the magnet, due to the cumulative magnetization effect of several magnetic nanoparticles entrapped within the same nanostructure.[29]

Considerable efforts have been undertaken by several groups in devising procedures for the controlled synthesis of polymer nanobeads encasing in their interior magnetic nanoparticles.[15,30−34] One challenge in this direction is to be able to control the size of the bead at the nanoscale, in order to preserve a high surface to volume ratio available for specific functionalization and consequently to achieve high sensitivity toward specific targets.[35] Additionally, providing the magnetic

*Address correspondence to teresa.pellegrino@unisalento.it.

Received for review October 14, 2010 and accepted December 22, 2010.

Published online January 10, 2011
10.1021/nn102761t

beads with fluorescent tags allows for multiplexing detection in combination with cell separation capabilities. QDs are ideal candidates as fluorescent tags for this purpose, due to their broad absorption spectra, their narrow emission band (which allows the use of a single light source for exciting at once various QDs emitting at different wavelengths), their high fluorescence quantum yield, and their robustness against photobleaching.[36]

The clustering of nanoparticles into an appropriate nontoxic polymeric bead is an appealing approach to multifunctional nanovectors for biomedical applications, also because the encapsulation of QDs within the polymer matrix preserves the QDs' fluorescence over a prolonged time[37−39] and at the same time the toxicity effects of the QDs are mitigated by their encapsulation layer.[40,41] Additionally, the polymer molecules can be easily functionalized with desired ligands for specific cell recognition.

We report here a procedure for fabricating multifunctional magnetic−fluorescent nanobeads (MFNBs) made of poly(maleic anhydride-*alt*-1-octadecene) by embedding both superparamagnetic manganese iron oxide nanoparticles (MNPs) and core−shell CdSe/ZnS nanocrystals (QDs), and we demonstrate a control over bead diameter from 70 to 160 nm. The nanobeads are formed by adding a destabilizing solvent to a starting solution of polymer and nanoparticles, which induces controlled aggregation of the components. A careful choice of this solvent allows tuning both the total bead size and the geometry of the beads in terms of nanoparticle distributions within the polymer, while the fluorescence signal of the nanobeads can be tuned by varying the relative ratio of fluorescent to magnetic nanoparticles added (QD:MNP).

Furthermore, we have chosen to decorate the surface of these MFNBs with folic acid molecules, which represents the third functionality in our system fulfilling the biorecognition task toward cell lines overexpressing folate receptors. To link such molecules, we have exploited the carboxyl groups present at the surface of the beads to bind folic acid (FA) bearing an amino spacer attached to it. The specificity of the FA-functionalized MFNBs toward human nasopharyngeal epidermal carcinoma (KB) cells was proven by detecting the fluorescence signal of the QDs embedded within the bead *via* confocal microscopy. Additionally, the high transmission electron micrograph (TEM) contrast of inorganic materials has allowed imaging with high precision of the localization of the FA-functionalized MFNBs on a TEM section of KB cells. Quantitative separation experiments of cells targeted *via* FA-functionalized nanobeads have been carried out in order to evaluate the efficacy of the FA-functionalized MFNBs in cell sorting applications.

RESULTS AND DISCUSSION

Synthesis of Magnetic−Fluorescent Nanobeads (MFNBs). For the preparation of MFNBs, first the MNPs and QDs were mixed together with the polymer in tetrahydrofuran, followed by the addition of a nonsolvent, such as acetonitrile or water, at a controlled flow rate. Figure 1a−c displays TEMs of MFNBs prepared by keeping constant the number of magnetic nanoparticles and by varying either the ratio of QD:MNP added or the destabilizing agent used. The ratio of quantum dots to magnetic nanoparticles (QD:MNP) inserted was 20:1 for the sample displayed in Figure 1a and 2:1 for the samples displayed in Figure 1b and c. Also, the nanobeads shown in Figure 1a and b were synthesized using acetonitrile as destabilization agent, while the sample shown in Figure 1c was synthesized using water as destabilization agent.

A closer look at the TEM images of the beads revealed the structural differences of the beads obtained by varying the preparation conditions. When acetonitrile was used as solvent and a QD:MNP ratio of 20:1 was employed (Figure 1a), the MNPs (with diameters around 9 nm) were clustered together and localized often in the central regions of the beads, while the QDs (the smaller dots with diameters around 3.5 nm) were more homogeneously distributed all over the volume of the beads (under TEM, the difference in diameters between the MNPs and the QDs helps to identify the distinct nanoparticles within the bead).

A similar distribution of nanoparticles inside the beads was observed when employing again acetonitrile as destabilizing solvent, but using a tenth of the amount of QDs as in the previous sample (*i.e.*, a QD:MNP ratio equal to 2:1, see Figure 1b), even if in this case much fewer QDs were found per bead. More generally, by using acetonitrile as destabilizing agent, the distribution of nanoparticles in the beads did not depend on the QD:MNP ratios, and the magnetic particles were always aggregated, while the QDs were distributed homogenously inside the bead (Figure 2b shows additional examples). In the case of acetonitrile-destabilized beads, the beads were quantitatively attracted to the magnet within three to six hours.

Alternatively, when water was used as destabilizing agent (Figure 1c) and a 2:1 ratio of QD:MNP was chosen, both the QDs and the MNPs were randomly distributed inside the bead. However, in this case, only a few MNPs and QDs were embedded within the same bead structure, with respect to the destabilization performed with acetonitrile.

The fewer MNPs present per bead likely accounted for the longer times needed for accumulation of the water-destabilized nanobead when placed close to a magnet (1−2 days). Additionally, the lower magnetic attraction of the water-destabilized nanobeads accounted also for a less effective magnetic separation: even after applying twice the magnet for recovering the MFNBs and for separating them from the side product of the reaction, free additional QDs were always found on the TEM carbon grid.

It is also worth noting that due to the solvent evaporation the nanobeads on the TEM grid appear close to each other and in some cases the beads are connected to each other through polymer filaments (Figure 1b and c). These

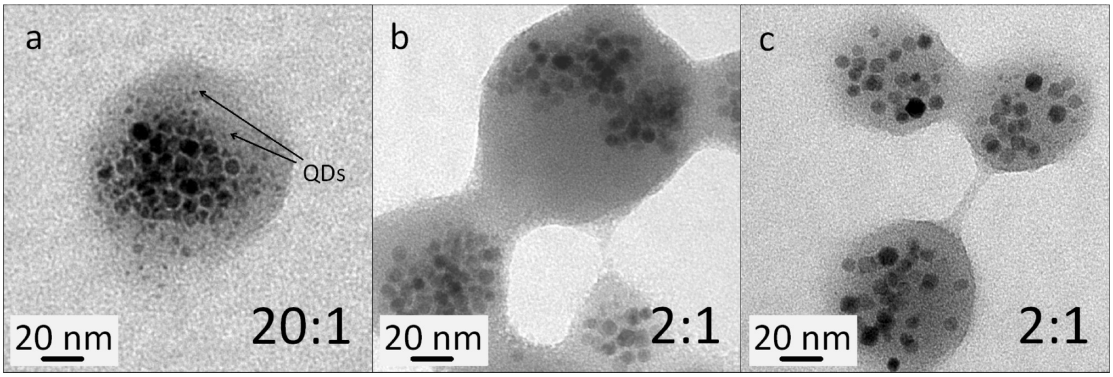

Figure 1. Transmission electron micrographs (TEM) of magnetic fluorescent nanobeads (MFNBs) prepared by varying either the ratio QD:MNP or the destabilizing solvent. The samples a and b were destabilized with acetonitrile, at QD:MNP ratios equal to 20:1 and 2:1, respectively. The sample c was destabilized by the addition of water and a ratio of QD:MNP equal to 2:1. In all the experiments the initial amount of MNPs was 0.1 nmol. (For a TEM overview at low magnification of these samples, see also Figure SI 3, SI.)

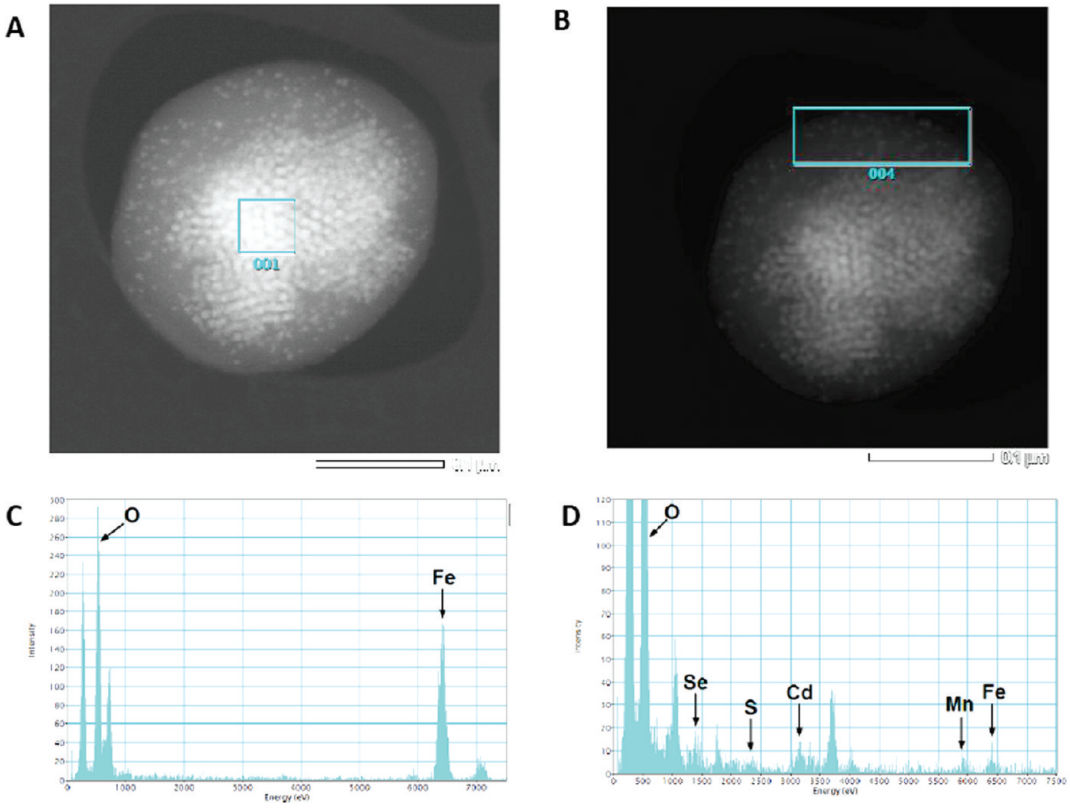

Figure 2. Cryo scanning transmission (STEM) images of a single bead prepared by destabilization with acetonitrile. In a and b two regions of interest, highlighted in aqua, one at the center (a) and the other on the bead shell (b), were selected for the compositional mapping as shown in c and d, respectively.

images might be misinterpreted, as they could be considered as reflecting the status of the beads in solution. However, the corresponding DLS sizes give a clear indication of the well-dispersed status of the beads in solution (see Figure SI 3, SI).

In order to confirm the QDs and MNPs distribution, not only based on the difference in size of the MNPs (9 nm) with respect to the QDs (3−4 nm) on the low-resolution TEM images, compositional profiling on a single bead prepared by destabilization with acetonitrile was performed *via* spatially resolved energy dispersive X-ray spectroscopy (EDS, see Figure 2). It was observed that in the bead center the iron (Fe) and oxygen (O) were the main elements that contribute to the bead composition. On the other hand in the bead shell, Cd, S, Se, and Zn were detected: the Fe peak, still present, was much less significant than in the central region (Figure 2c and d and Table 1S of the SI for compositional percentage summary).

The observed different morphologies of the nanobeads prepared using respectively water or acetonitrile

as destabilizing agents can be explained looking at the stability of the individual components in the conditions in which the beads are formed. The QDs were slightly more stable with respect to addition of acetonitrile than the MNPs, likely due to their smaller size and to the presence of different surfactants at their surface (TOPO and TOP on QDs with respect to oleic acid and oleylamine for the MNPs). Thus, when the acetonitrile was added, first the MNPs clustered together forming small aggregates, followed by a relatively simultaneous condensation of the QDs and of the polymer around these MNP aggregates. When instead water was added to the system, the polarity of the solvent increased drastically, and consequently the polymer condensed so rapidly into nanobeads that the MNPs did not have enough time to arrange in seed clusters, as when using acetonitrile. This was likely due to the poor solubility in water of the polymer, which resulted in its fast shrinkage.[32] Hence, in this case many more (and thus smaller) nanobeads were formed than in the acetonitrile case. During the nanobead formation from water destabilization, the polymer entrapped randomly both the QDs and the MNPs, and these nanoparticles were spread relatively homogeneously all over the nanobead. Control experiments in which only QDs or MNPs or just polymer was present confirmed the different behavior of each component (data not shown).

Depending on the preparation parameters, the overall diameter of the MFNBs could be varied, as statistically determined by TEM (for size distributions see also SI Figure SI 2). In the case of acetonitrile, the mean diameters remained around 80 $\pm$ 40 nm for small ratios of QD:MNP, while for high QD:MNP ratios, *i.e.*, 40:1, corresponding to larger amounts of QDs inserted into the bead structures, the average bead size increased up to 120 $\pm$ 46 nm. In the case of nanobeads prepared by water destabilization, the mean bead diameters were significantly smaller, with an average diameter tunable between 58 and 73 nm (with a standard deviations of 10−20%) and still dependent on the QD:MNP ratio used, as shown in Figure 1c (see also Figure S2, SI).

The average size of the nanobeads, prepared in the different conditions above-described, was also estimated by DLS measurements (see Figure S3, SI). As expected, the mean diameters measured by DLS are larger than those estimated by TEM since the nanobeads in solution are hydrated (the peaks are centered at values around 100 nm for the sample prepared by using water as destabilizing agent and at 200 nm for the sample prepared by using acetonitrile). Additionally, the full-width half-maximum values (between 60 and 120 nm) together with the low polydispersity indexes recorded indicate the absence of aggregates in solution for the samples obtained by this method.

The photoluminescence (PL) spectra of the bead samples prepared by acetonitrile destabilization, shown in Figure 3a, were recorded at an excitation wavelength

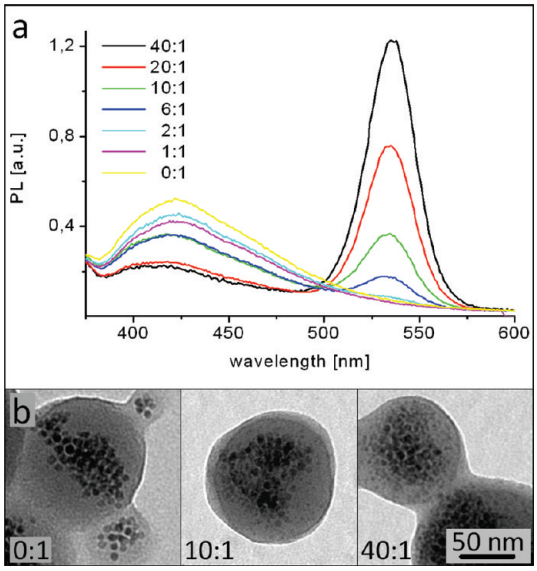

Figure 3. Photoluminescence spectra (a) of the acetonitrile-destabilized MFNBs. The QD:MNP ratio was varied from 0:1 to 1:1, 2:1, 6:1, 10:1, 20:1, and 40:1. The amount of MNP was kept constant at 0.1 nmol in all cases, whereas the amount of QDs was varied from 0 nmol to 4 nmol. Higher magnified TEM images of beads obtained with a QD:MNP ratio of 0:1 (left), 10:1 (center), and 40:1 nmol (right) are shown on the bottom (b).

of 350 nm, and the concentration of the samples was adjusted in a way that the optical density of all samples was equal to 1.22 at 350 nm. In order to draw quantitative conclusions from the emission spectra, the following assumptions have to be made: (a) the photoluminescence quantum yield of the quantum dots remains constant in all cases (which is reasonable, since the QDs were treated completely equally in all cases); (b) the influence of the magnetic particles on the emission is the same in all samples (which is reasonable since the concentration of magnetic particles is kept constant at 0.1 nmol; see also SI Figure SI 4); (c) the scattering behavior of all samples is similar, which is reasonable for all but less for the sample with the highest QD concentration, since in all other samples the contribution of the QD absorption to the optical density of the sample is negligibly low and the optical density is the same for all samples at the excitation wavelength.

Under all these assumptions, the emission signal from the QDs (at 533 nm) is proportional to the concentration of QDs in the sample. The emission signal of the nanobeads significantly increases when larger amounts of quantum dots are used in the bead synthesis (Figure 3a), and the amount of quantum dots incorporated into the nanobeads scales with the amount of quantum dots used for the nanobead synthesis, as found by TEM investigations (Figure 3b).

Additionally, in support of these results also elemental analysis on these samples confirms the increasing ratio of Se to Fe found whenever a higher QD:MNP ratio was inserted (Table S2, SI).

Furthermore, the luminescence signal at 533 nm that is originating from the band gap luminescence of the CdSe/ZnS QDs remains unchanged in position and shape when comparing the spectra at different QD:MNP ratios as well as when comparing the spectrum of the original as-synthesized QDs in toluene with the spectrum of the magnetic luminescent nanobeads. This finding allows the conclusion that in the examined systems QD−QD interactions as well as QD−MNP interactions are negligible with respect to the optical properties of the QDs.

Another finding is that the additional luminescence peak, with its maximum around 420 nm (which is attributed to luminescence of the polymer), decreases with increasing amount of QDs inserted. One possible explanation for this behavior might be attributed to fluorescence energy transfer (FRET) between the QDs and the polymer. Since the QDs have a high extinction coefficient at the emission wavelength of the polymer and are closely surrounded by the blue-emitting polymer, a resonant energy transfer from the polymer to the QDs is conceivable (FRET efficiency depends mainly on the overlap of the emission spectrum of the donor and the absorption spectrum of the acceptor and on the distance between donor and acceptor). This would result in a quenching of the photoluminescence of the polymer and an increase of the PL of the QDs in the system, matching the observed luminescence behavior shown in Figure 3a. Indeed, FRET processes have been demonstrated from dyes to QDs on various systems recently.[42−44] It should be mentioned that the relatively weaker luminescence from the polymer at higher quantum dot concentrations might also originate from an overall lower polymer concentration. The obtained nanobeads are slightly bigger when higher amounts of QDs are inserted (see discussion in the SI) and thus have a larger scattering cross section per volume. Since for the PL measurements all the samples have the same optical density at the excitation wavelength, this would result in a slightly lower polymer concentration for the samples with more QD loading (and thus a larger diameter). A lower polymer concentration would result in a lower PL signal from the polymer (at 420 nm) even in the absence of a FRET mechanism. However, if this is the case, the fluorescence intensity (and hence the concentration) of the nanobeads (of the QDs as well as of the polymer) with higher QD concentration would even have been underestimated in our measurements. Summarizing, the trend of the weaker fluorescence signal of the polymer (420 nm) with rising QD concentration could be assigned either to a FRET process from the polymer to the QDs or to a systematic underestimation of the bead concentration in the samples with higher QD:MNP ratios.

Even for the samples destabilized by water it was possible to tune the fluorescence of the beads by varying the QD:MNP ratio (Figure SI 5, SI). In this case, however, one should be aware that even for the twice washed nanobeads it was not possible to exclude the presence of free QDs, which were difficult to separate from the nanobeads, and therefore a quantitative evaluation of the recorded PL spectra is not ensured (Figure SI 4, SI).

Furthermore, it should be mentioned that the extinction spectra of the nanobead samples obtained by using either acetonitrile or water as destabilizing agents, besides showing the typical absorption bands of the QDs employed, additionally revealed a scattering component caused by Mie scattering of the nanobeads (Figure S7, SI), as expected for objects of this size range.

Finally, it should be pointed out that even after several months of storage at room temperature (25 °C, in the dark) the luminescence of the MFNBs was preserved (this could be observed even by the eye; see Figure SI 8).

Preparation of FA-EBE-NH_2. The surface of the as-synthesized MFNBs is uniformly covered with carboxyl groups deriving from the hydrolysis of the polymeric maleic anhydride. These groups are highly reactive toward nucleophiles and can be exploited to attach amine-functionalized compounds, thus yielding very stable amide bonds. In particular, in our case we decided to equip the folic acid molecule with a biocompatible linker featuring a terminal primary amine, which could be reacted with the polymer. Folic acid already presents a primary amine in its structure; however it is an aromatic amine and thus less reactive toward nucleophiles. A common approach already reported in the literature involves the functionalization of the γ-COOH group of the FA molecule in order to graft different groups suitable for further conjugations.[45] As highlighted in Scheme 1, our strategy was to prepare an amine-modified folic acid by means of a short biocompatible linker, namely, 2,2′-(ethylenedioxy)bis(ethylamine) (EBE). In order to reduce the amount of byproduct and improve the total yield of the reaction scheme, one of the two amines of the EBE molecules was temporarily protected with Fmoc, which could be subsequently removed under mild basic conditions (Scheme 1B). Fmoc-Cl was reacted with the diamine linker used to obtain the monoprotection. The different solubility of the products in the reaction mixture was exploited to purify the desired compound by a series of acidic and basic washing steps, after which both thin-layer chromatography (TLC) and electrospray ionization mass spectrometry (ESI-MS) confirmed the preparation of pure Fmoc-EBE-NH_2 (see Figure SI 9, SI) and the removal of unreacted products. It should be mentioned that traces of the bis-protected compound were also observed by mass spectroscopy, even though this compound does not interfere with the subsequent reaction steps (the peak at 593 on the ESI-MS spectra; see Figure SI 10, SI).

To activate the carboxyl group of folic acid for the conjugation with the protected linker, the *N*-hydroxysuccinimide ester of the folic acid was prepared (Scheme 1A),

Scheme 1. Reaction Scheme for the Synthesis of Amine-Modified Folic Acid[a]

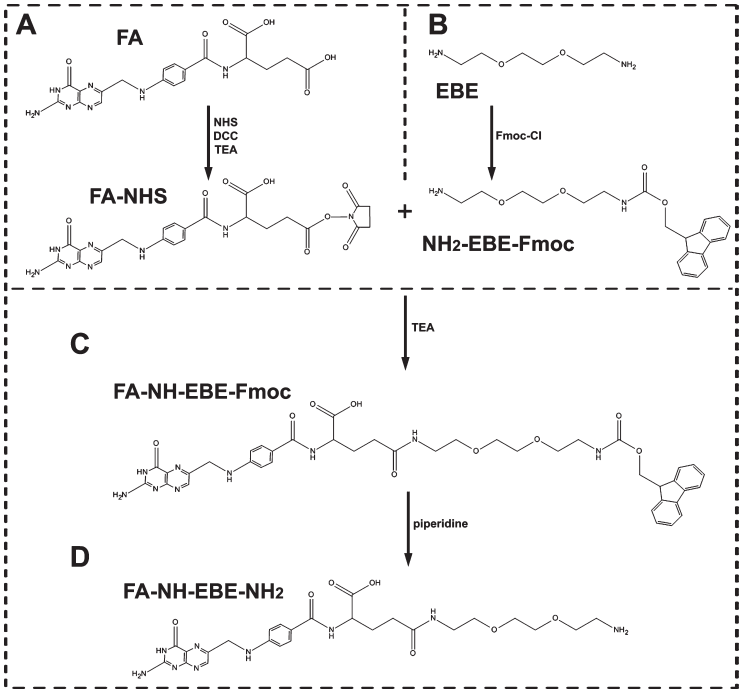

[a] Starting with the preparation of NHS-activated folic acid (A) and monoprotected Fmoc-EBE (B) we reacted the FA-NHS produced in reaction A with the NH_2-EBE-Fmoc produced in reaction B to prepare Fmoc-EBE-NH-FA (C). Subsequently we de-protected the amino group (D), which was then available for linkage to the nanobead surface.

following a protocol already reported in the literature.[45] The formation of a water-insoluble byproduct, the dicyclohexylurea, confirmed the successful reaction between the carboxylic group and the free primary amine of the linker, as also reported by Sonvico *et al.*[45]

After purification, the activated folic acid was reacted with the as-synthesized Fmoc-EBE-NH_2 (Scheme 1C). The reaction was carried out in dimethyl sulfoxide (DMSO) without the need of any further coupling agent, due to the high reactivity of the amine toward the hydroxysuccinimide ester.

After several washing steps of the reaction product with cold anhydrous diethyl ether, an oily product was obtained, which corresponded to FA-NH-EBE-Fmoc, as confirmed by mass spectrometry (see Figure SI 11, SI).

In order to obtain the final product, the amine-functionalized folic acid, piperidine was added to the mixture in dimethylformamide (DMF), thus removing the Fmoc protecting group, and the amino-terminated folic acid (FA-NH-EBE-NH_2) was recovered ready for the attachment to the nanobeads (Scheme 1D). Even in this case the deprotection was further confirmed by mass spectrometry (see Figure SI 12, SI).

Functionalization of the Nanobeads with Folic Acid. As discussed above, the surface of the MFNBs was functionalized, promoting the formation of an amide bond between the carboxylic groups of the polymer and the aliphatic amine of linker-functionalized folic acid molecule *via* activation of the carboxyl group with a carbodiimide, namely, EDC. The functionalization of the nanobeads was monitored by zeta-potential measurements. Although the number of negative charges, *e.g.*, carboxylic groups, remained unchanged after conjugation of each folic acid molecule grafted to the nanobeads (after coupling reaction of the folic acid to EBE, one of the two carboxyl groups of folic acid contributes to the charge, while the other one is used in the linking procedure), a new primary amine per each folic molecule attached was added to the surface of the nanobead, thus increasing positively the net electrical charge of the derivative. This led to a significant change of the dependence of the nanobead surface charge on the pH. Indeed, while the as-synthesized nanobeads had a net variation of charge at almost pH 5.5 (likely assigned to the protonation of the carboxylic groups when the pH is lowered), the FA-functionalized nanobeads showed a charge shift at a pH of about 7.5 (Figure 4) (in this case, this value might likely be assigned to the protonation of the amino groups of the folic molecules). Besides, both in the protonated state and in the deprotonated one, the overall charge of the FA-functionalized nanobeads (FA-MFNBs) was always more negative than the corresponding nonfunctionalized nanobeads. It is worth noting that no significant change of the DLS diameter of the nanobeads was observed after folic acid functionalization, most likely due to the small size of the FA-NH-EBE-NH_2.

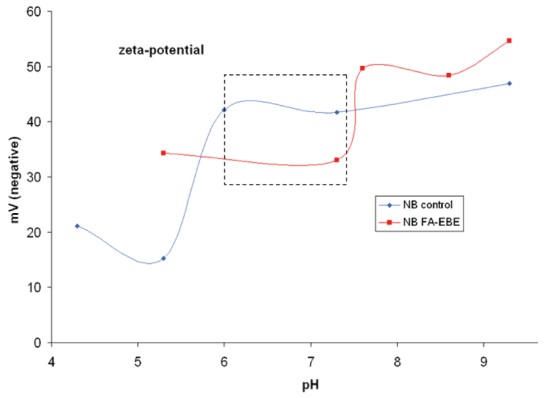

Figure 4. Modification of the charge surface of the folic acid nanobeads (FA-NBs) with respect to the starting nonfunctionalized nanobeads. The surface potential versus pH is plotted for the starting nanobeads (blue curve) with respect to the FA-MFNBs (red curve).The pH at which a net shift of the charge is recorded for the starting nanobeads corresponds to 5.5, while that of the FA-MFNBs is shifted at pH 7.5 (the lines are drawn in order to guide the eyes).

In addition to the nanobead stability at the different values of pH tested in the zeta-potential analysis, the behavior of the FA-MFNB in cell culture medium (RPMI-1640) was investigated by monitoring the hydrodynamic diameter. The average DLS diameter was not altered significantly over 90 min (Figure SI 13, SI). Furthermore, the functionalized nanobeads could be stored at 4 °C for months without exhibiting any stability problems.

Cellular Studies. In order to demonstrate the potential biomedical application of FA-MFNBs, first the uptake experiments were carried out on a cancer cell line, namely, KB, which overexpresses the α1 isoform of the folic acid receptor. To facilitate the interaction between the FA-MFNBs and the cells at very low nanobead concentration (32 μg/mL of Fe, which corresponds to a concentration of 50 nM for $MnFe_2O_4$ nanoparticles of 8 nm in diameter), the cells in suspension were shaken with FA-MFNBs at 37 °C for 1 h.

After incubation, a drop of the targeted cells that were separated by a magnet was cast on a glass slide and analyzed under a confocal microscope. Clear evidence of the successful quantitative uptake of the FA-MFNBs was observed (Figure 5a). By analyzing the cell suspension along the *z*-axis, with a zeta step of 5 μm, it was possible to confirm the intracellular localization of the FA-MFNBs up-taken (Figure 5b and Figure SI 14 for TEM characterization as explained later). The FA-MFNBs were mainly found in the cytoplasm of the cells, as the fluorescent spots were evident in the sections in which the nuclei were also well in focus and only partially attached to the cellular membrane. Also, competitive FA-MFNB uptake assays in the presence of free folic acid have been performed. As observed by confocal analysis, after 60 min at 37 °C the presence of free folic acid in solution caused a significant decrease in the binding of the FA-MFNBs to the cells, thus supporting the receptor-mediated endocytosis pathway (Figure SI 17, SI).

As an additional control, when using polyethylene glycol functionalized MFNBs (PEG-MFNBs), which therefore did not carry folic acid molecules at their surface, while keeping all the other experimental conditions as in the previous experiment, no fluorescence signal was observed in the cells after the same time lapse (Figure SI 18, SI).

To further understand the intracellular uptake process of FA-MFNBs, TEM analysis was performed on doped KB cells at different time delays (Figure 6). After 20 min of incubation at 37 °C, the MFNBs having a strong TEM contrast (and thus appearing as black spots with respect to the cell) were mainly localized at the cell membrane, and only a few of them were already observed in early endosome vesicles (Figure 6a). Indeed, after 60 min the FA-MFNBs up-taken were identified in several early and late endosomes (Figure 6b). Interestingly, as evidence of the receptor-mediated endocytosis due to the folic acid−folate receptors recognition, the FA-MFNBs were arranged as a crown on the inner membrane of almost all the endosomes (no beads were found in the center of the endosome, but instead they were attached exclusively to the endosome contour; see Figure 6b and c). Furthermore, the localization was exclusively cytoplasmatic, and no FA-MFNBs were observed in the nuclei of the doped cells (for an overview see Figure SI 14, SI), indicating once more an endocytosis pathway. As an additional confirmation of the endocytosis pathway followed by the FA-MFNBs, in a control cell uptake experiment performed at 4 °C after 1 h of incubation, we observed the beads only at the cell surface, thus excluding other possible cellular uptake pathways (Figure SI 15, SI). As observed in a control experiment, the PEG-MFNBs were not up-taken by the cells, as indeed no beads were observed in the entire cell control (Figure SI 16, SI). It is worth mentioning that under the incubation conditions used no sign of cell suffering or morphological changes was observed by TEM (see Figure 6 and Figure SI 14, SI).

The TEM cell characterization also suggested the possibility of reducing even the incubation time for achieving specific folate-mediated recognition, since within the first 20 min of incubation the beads were already attached to the cell surface. We also compared two distinct cell lines, namely, the KB cells already mentioned and the MCF7, which is a breast cancer cell line that does not overexpress folate receptors but takes up folate at a basal level.[45] After 20 min of incubation, we could identify qualitatively, by confocal analysis, their different uptake of folate nanobeads. The fluorescence signal was by far higher in KB cells than in the corresponding MCF7 under the same imaging parameters, thus confirming the selectivity achieved with our FA-MFNBs (Figure SI 19, SI). In the control experiment, namely, after incubating nonfunctionalized nanobeads

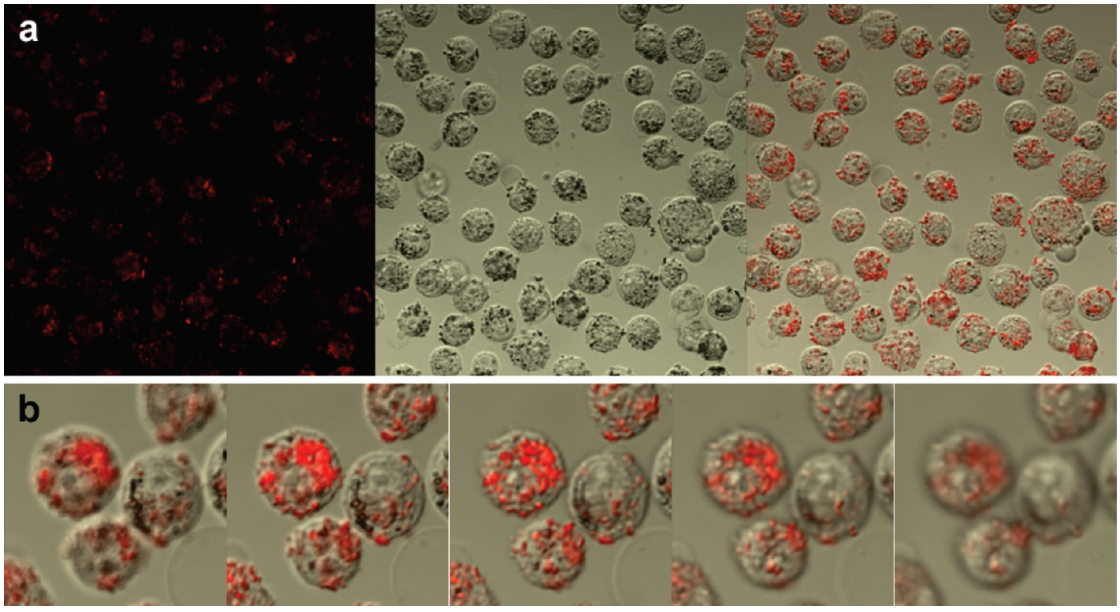

Figure 5. Confocal images of KB cells targeted with folic acid functionalized nanobeads (FA-MFNBs). After 1 h of incubation at 37 °C with nanobeads at a Fe concentration of 32 μg/mL, the cells showed many fluorescent spots (panel A). The zeta stack analysis (5 μm slices) confirmed the internalization of the nanobeads in the cell cytoplasm (panel B).

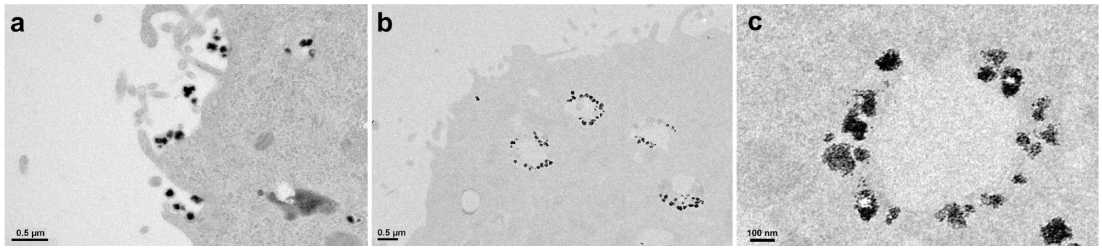

Figure 6. TEM images of KB cells doped with FA-MFNBs. The cells were treated with FA-MFNBs at 37 °C for 20 min (a) and 60 min (b and c), respectively. While after 20 min the nanobeads were more localized close to the cell membrane and only a few early endosomes were present, after 60 min the FA-MFNB up-taken could be identified in several early and late endosomes. By looking closer at the vesicles (c) the MFNBs were found to decorate the bead vesicle walls, thus confirming the receptor mediated endocytosis process mediated by the folic acid.

(*i.e.*, the EBE-MFNBs) for 20 min, we did not observe any significant signal.

In a previous work,[32] we have shown the accumulation on a 0.3 T magnet of cells that had been doped nonspecifically with magnetic beads (for 24 h at 37 °C). Such incubation time was required in order to ensure that the cells had up-taken by nonspecifically endocytosis enough nanobeads to respond to the magnet. Furthermore, MTT proliferation assay confirmed the low toxicity of the magnetic beads even when applied at the same doping concentration as the one used in this work (32.5 μg/mL). Additionally, several works have shown that although CdSe/ZnS QDs are made of toxic elements and their toxicity is strictly related to the Cd ion release, whenever the QDs are encapsulated within a matrix, their toxicity is significantly reduced (at least on a short time scale as the one used in our experiments) and the florescence of QDs can be kept for a longer time.[35,41,46,47] In the present study, besides having developed a system that is at the same time magnetic and fluorescent (thanks to the inclusion of magnetic nanoparticles and fluorescent QDs), the surface decoration of nanobeads with folic acid yielded a trifunctional probe possessing enhanced affinity toward tumor cells overexpressing folate receptors. The resulting FA-MFNBs can accomplish in only one hour (or even in 30 min) the specific targeting and sorting

TABLE 1. Summary of the Cell Sorting Assay Results[a]

% doped cells	% sorted cells
50	47.6 ± 3.7
25	25.1 ± 3.7
10	10.1 ± 0.4
5	5.5 ± 0.6
2.5	2.3 ± 0.2
1	1.0 ± 0.2

[a] On 100 000 total cells the fraction of doped cells corresponds to the % reported in the first column. The percentage of cells sorted to the magnet on such samples is reported in the second column. Each data point corresponds to the mean value of three independent experiments.

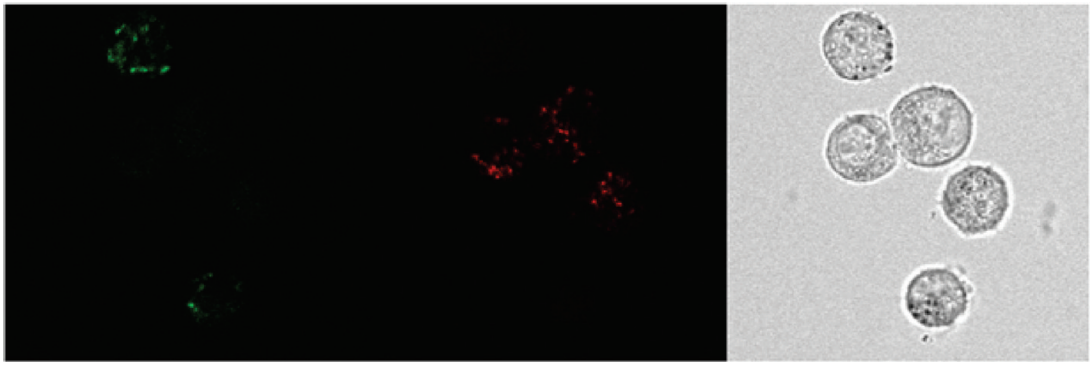

Figure 7. Confocal microscope analysis of KB cells doped with two FA-MFNB samples, prepared with different QD samples (green- or orange-emitting nanocrystals). The acquisition was performed using the same argon laser source emitting at 488 nm, and the fluorescence signals were recorded in 525 ± 15 nm (a) and 590 ± 15 nm (b) windows.

of KB cells. In addition, in the present work we have studied the recovery of small cellular fractions targeted with FA-MFNBs from a pool of nontargeted cells. The doped cells were mixed with control cells in defined ratios (50%, 25%, 10%, 5%, 2.5%, and 1% of doped cells) and were incubated at 37 °C for 60 min. A magnet was then placed closed to one side of the vial for 30 min. Thereafter, the cell suspension was removed and the portion attracted by the magnet was resuspended in a fresh phosphate buffer solution. By counting the fraction of cells in the supernatant and that at the magnet, it was possible to estimate the amount of doped cells that had been recovered. The results are summarized in Table 1. Remarkably, it was possible to recover with our system the entire initial fraction of doped cells even when using the lowest ratio (1% of doped cells). These results are in accordance with the cell recovering percentage reported in other studies using other magnetic systems on other cellular lineages.[48−50] These results open the opportunity to use this nanosystem for the isolation of small populations in a cell pool. As a proof that only doped cells had been recovered, in the 10% ratio experiment the two recovered portions were reseeded after the sorting. The adherent cells were analyzed under a confocal microscope after 16 h (Figure SI 20, SI). It was possible to collect fluorescence signal only from the sorted cells, while in the nonsorted cell sample there was no signal in the fluorescence window.

Finally, in order to investigate the feasibility of multiplexing analysis using FA-MFNBs, two different samples of QDs with different maximum emission wavelengths were also used for the synthesis of the nanobeads, thus obtaining two differently colored FA-MFNB types of nanobeads.

Two suspensions of KB cells were doped separately with the two MFNB-FA, emitting green and orange fluorescence, respectively. Thereafter, the doped suspensions were counted, and a solution was prepared by mixing 50% of each sample. This solution was analyzed by confocal microscopy, using a 488 nm argon laser source. As shown in Figure 7, it was possible to collect simultaneously the two fluorescence signals from the doped cells in the green and red channel, respectively. By confocal microscopy, emission profile spectra of the FA-MFNB taken up were recorded, with no significant modification from the original photoluminescence spectra (Figure SI 21, SI).

CONCLUSIONS

In summary, multifunctional polymer nanobeads containing MNPs and QDs have been synthesized by destabilization of a mixture of magnetic nanoparticles, quantum dots, and an amphiphilic polymer, followed by subsequent surface functionalization with folic acid. The luminescence of the resulting beads increased with increasing quantum dot concentration per bead. The distribution of the nanoparticles within the beads could be tuned using either water or acetonitrile as a destabilizing agent. When choosing acetonitrile, the MNPs were found clustered in the center of the bead, while the QDs were uniformly distributed all over the bead structure. Alternatively, by using water as destabilizing solvent, both the MNPs and the QDs were uniformly distributed all over the bead. The different geometries obtained affected the magnetic response: the acetonitrile-destabilized nanobeads reacted faster to an external magnetic field applied with respect to those obtained by using water as destabilizing agent. Therefore, the first ones were chosen for the cell sorting study carried out in this work.

The procedure developed for the preparation of magnetic−fluorescent nanobeads is fast and easy, since, especially in comparison to the copolymerization synthesis procedures for nano- and microspheres,[16,25,26] it is based on a one-pot synthesis and at the same time is cost-efficient, as the polymer used is indeed commercially available.

Furthermore, the surface of the nanobeads was functionalized with folic acid. The enhanced uptake of these nanobeads by cancer cells overexpressing folate receptors was demonstrated. Due to the fast magnetic accumulation and still high surface to volume ratio in

these 100 nm beads, highly efficient cell separation was possible, even at a low percentage of the targeted cells with respect to nontargeted ones. Confocal measurements of the separated cancer cells revealed the specificity of the FA-functionalized nanobeads, and TEM characterization of the cells suggested a receptor-mediated uptake mechanism. Provided the proof of concept for application of this trifunctional nanosystem in cell sorting experiments, it will be significant to test it on clinical samples in a further study.

MATERIALS AND METHODS

Chemicals. Milli-Q water (18.2 MΩ, filtered with filter pore size 0.22 μM) was from Millipore. Acetonitrile was from T.J. Baker, Ultra Gradient HPLC grade. Tetrahydrofuran anhydride was from Carlo Erba, p.a. Poly(maleic anhydride-*alt*-1-octadecene), M_n 30 000−50 000, iron(acetylacetonate)$_3$, manganese(acetylacetonate)$_2$, hexadecanediol, dodecylamine, dodecanoic acid, benzyl ether, 2,2′-(ethylenedioxy)bis(ethylamine) (EBE), *N*-hydroxysuccinimide (NHS), *N*-(3-dimethylaminopropyl)-*N*′-ethylcarbodiimide hydrochloride (EDC), folic acid (FA), triethylamine (TEA), DMSO, DMF, diethyl ether, piperidine, Dulbecco's modified Eagle's medium (DMEM), fetal bovine serum (FBS), glutamine, penicilline/streptomicine, glutaraldehyde, sodium cacodylate trihydrate, osmium tetroxide, and epoxy resin were purchased from Aldrich. *N*-Hydroxysuccinimide (NHS) was purchased from Pierce. RPMI-1640 without folic acid was purchased from Euroclone.

Synthesis of Luminescent and Magnetic Nanobeads. For the preparation of MFNBs, 0.1 nmol of manganese iron oxide nanoparticles (see Supporting Information, Figure S1),[51] 0.1 nmol (or 0.2, 0.6, 1, 2, and 4 nmol) of cadmium selenide-zinc sulfide core−shell quantum dots[52,53] (QDs) (Figure S1, SI) and poly(maleic anhydride-*alt*-1-octadecene) (1.5 μmol monomer units) were dissolved in 200 μL of tetrahydrofuran in an open 8 mL glass vial. The mixture was shaken for 30 min (1000 rpm shaking rate). Then, 0.8 mL of acetonitrile or water was added dropwise at a flow rate of 250 μL/min. After the bead formation, the sample was cleaned twice by placing it onto a permanent magnet overnight, followed by redispersion of the beads in fresh water (see also SI for more details).

Photoluminescence Spectra. The luminescence spectra of twice washed beads were recorded using a 1 mL quartz cuvette in a CARY Eclipse (Varian) photoluminescence spectrometer after adjusting the sample concentrations so that the optical densities at the excitation wavelength were equal in all cases (1.22 and 0.98 for samples synthesized using acetonitrile or water, respectively). This was performed in order to achieve similar excitation conditions, since in the present samples the scattering of relatively similarly sized samples dominates over the absorption of the quantum dots (assuming constant absorption of the magnetic nanoparticles). For higher QD contents, however, the error due to this approximation is expected to be larger, since not only the absorption of the QD becomes significant but also the bead size increases, which again influences the scattering properties of the nanobeads. The excitation wavelength chosen was 350 nm. In addition to the excitation filter (250−395 nm), a UG11 (Schott) filter with a transmittance of around 0.90 at 350 nm and very low transmittance in the visible was inserted into the excitation beam. Furthermore, the following setup parameters were chosen: emission filter 360−1100 nm, emission slit 5 nm, excitation slit 10, 5, or 2.5 nm (comparison using a dilute rhodamine 6G solution as a fluorescence standard), scan rate 120 nm/min, average time 0.5 s, PMT detector voltage 850 V.

Dynamic Light Scattering. Dynamic light scattering (DLS) was performed using a Zeta Sizer (Malvern Instruments) equipped with a 4.0 mW He−Ne laser operating at 633 nm and an Avalanche photodiode detector, in order to determine the average size of the nanobeads (for DLS data please see the Supporting Information).

Elemental Analysis. The concentration of the iron and selenium content in the cleaned bead dispersions was determined by elemental analysis using an ICP-AES spectrometer (iCAP 6500, Thermo) (for ICP-AES data, see the Supporting Information).

Mass Spectrometry. Mass spectrometry analyses were performed on an Agilent 1200 Series HPLC, equipped with Agilent 6300 Series ion trap LC/MS systems. For the ionization of the analyzed compounds, electrospray ionization (ESI) or atmospheric pressure chemical ionization (APCI) sources were used.

Confocal Microscopy. Confocal microscopy images were acquired by a Nikon Eclipse Ti microscope equipped with an argon laser source (excitation at 488 nm). Images were recorded using an acquisition window set at 525 ± 15 nm for the green-emitting QDs and 590 ± 15 nm for the orange-emitting QDs.

Transmission Electron Microscopy and STEM/EDX CRYO Analysis. The sample vitrification procedure was carried out by depositing 3 μL of the sample in water on a holey carbon film grid (200 mesh, HC200-Cu EMS) using a homemade cryo-plunger. Before depositing the sample the grids were plasma-treated using a Gatan Solarus 950 plasma cleaner in order to render them more hydrophilic. The cryo scanning transmission electron microscopy (STEM) images were acquired in a Jeol JEM 2200FS equipped with a field-emission gun (FEG) operating at 200 kV. A Gatan cryo-holder operating at −175 °C was used. The images were recorded using a 1k _ 1k Gatan charge-coupled device (CCD) camera.The Z-contrast STEM measurements were acquired using a 0.2−0.5 nm probe size beam and recording the images with a high-angle annular dark field detector (HAADF) and a camera length of 50 cm. The data were gathered using for both TEM and STEM analyses a low electron dose in order to avoid beam damage of the sample and preserve the vitrified aqueous film.

The chemical analysis of the nanostructures was carried out with a JED-2300 energy dispersive X-ray spectrometer using a 0.5 nm probe size beam scanned on the samples (STEM) and acquiring X-ray spectra at each point of the scan. The chemical quantification was performed using the Cliff−Lorimer method, which is considered as a good approximation for thin materials.

Preparation of Amine-Modified Folic Acid (FA-EBE-NH$_2$). To functionalize the nanobead surface with folic acid molecules, a short linker, 2,2′-(ethylenedioxy)bis(ethylamine) (EBE), was used. In detail, 0.4 mmol of EBE was dissolved in 8 mL of anhydrous $CHCl_3$ in a round-bottom flask under nitrogen. Then, in order to temporarily protect one of the two amines, 0.2 mmol of 9-fluorenylmethoxycarbonyl chloride (Fmoc-Cl) in 2 mL of anhydrous $CHCl_3$ was slowly added over a time lapse of 20 min. The temperature of the mixture was kept at 0 °C for 1 h, then at room temperature overnight. The resulting mixture was transferred into a separatory funnel and washed with 20 mL of a NaCl solution (5 M), 1 mL of NaOH (1 M), and again four times with 20 mL of a NaCl solution (5 M). The complete removal of byproduct after the washing steps was checked by thin-layer chromatography (TLC) on silica plates (mobile phase: 10% CH_3OH in CH_2Cl_2). The organic phase was extracted, the solvent removed *in vacuo*, and the residue (the product Fmoc-EBE-NH$_2$) dissolved in fresh $CHCl_3$ to obtain a 50 mM solution (as determined *via* gravimetric analysis).

To conjugate the folic acid molecule with Fmoc-EBE-NH$_2$, FA was activated by means of *N*-hydroxysuccinimide (NHS) by following a protocol published by Sonvico *et al.*,[45] with minor modifications. Briefly, FA (100 mg, 0.22 mmol), TEA (48 μL, 0.34 mmol), and anhydrous DMSO (1.5 mL) were mixed in a round-bottom flask under N_2. A solution of NHS (52 mg, 0.45 mmol) and *N*,*N*′-dicyclohexylcarbodiimide (DCC, 93 mg, 0.45 mmol) in

anhydrous DMSO (0.5 mL) was injected, and the mixture was vigorously stirred overnight at room temperature in the absence of light. The solution was filtered on a syringe membrane (0.22 μm cutoff size), thus removing the byproduct dicyclohexylurea, and the product was recrystallized from cold anhydrous diethyl ether (Et_2O). The purified NHS-FA was dissolved in anhydrous DMSO in order to obtain a 50 mM solution (gravimetric analysis).

To obtain FA-EBE-Fmoc, 1 mL of 50 mM EBE-Fmoc in $CHCl_3$ (0.05 mmol) was injected into a vial, and the solvent was removed by a gentle nitrogen flow. Then, 1 mL of 50 mM NHS-FA in DMSO (0.05 mmol), 4 mL of anhydrous DMSO, and 150 μL of TEA (1 mmol) were added, and the mixture was stirred overnight at room temperature. The solution was washed with cold anhydrous diethyl ether to yield the product as an oil.

To obtain the final compound FA-EBE-NH_2, FA-EBE-Fmoc was dissolved in piperidine (2 mL of a 20% solution in dimethylformamide) and the mixture stirred for 1 h. The solution was washed several times with cold anhydrous diethyl ether and finally dissolved in anhydrous DMSO in order to obtain a 10 mM solution (gravimetric analysis).

Functionalization of Magnetic Fluorescent Nanobeads with FA-EBE-NH_2 (FA-MFNBs). To functionalize the surface of the as-synthesized nanobeads with the amine-modified folic acid, a 10-fold batch of magnetic fluorescent nanobeads was diluted in 2 mL of sodium borate buffer (50 mM, pH 9) and mixed with 10 μL of TEA (71 μmol), 200 μL of 10 mM FA-EBE-NH_2 (2 μmol), and 1 mL of 0.4 M *N*-(3-dimethylaminopropyl)-*N*′-ethylcarbodiimide hydrochloride (EDC) in sodium buffer borate. The solution was mixed on an orbital shaker for 6 h at room temperature. The nanobeads were washed several times by adding ultrapure water and later removing it while attracting the nanobeads to the wall of the vial with a NdFeB magnet. The purified sample was finally dissolved to the desired concentration in phosphate buffer saline (PBS).

Cellular Studies. To investigate the potential biomedical application of FA-modified MFNBs, the KB cell line was used. This line derives from an epidermal carcinoma of the mouth, and it is well-known in the literature for overexpressing the alfa-1 isoform of folic acid receptor. KB cells were grown at 37 °C and under 5% CO_2 atmosphere in folate-free RPMI-1640 medium, supplemented with L-glutamine (2 mM), penicillin (100 units/mL), streptomycin (100 μg/mL), and 10% heat-inactivated fetal bovine serum.

To analyze the cellular uptake of FA-MFNBs by means of confocal microscopy, KB cells were detached from the flask with trypsin and counted. Therefore, 5×10^5 cells were dispersed in 0.5 mL of folate-free RPMI-1640, containing FA-MFNBs with 32.5 μg/mL metal ion concentration, and transferred into a glass vial. The suspension was gently mixed at 90 rpm on an orbital shaker at 37 °C for 20 min in one series of experiments or 1 h in the other series. The cells were then centrifuged, washed three times with PBS, and fixed with 4% paraformaldehyde for 10 min at room temperature. Finally, they were washed three times and suspended in PBS. The confocal microscope analysis was performed by casting a drop of fixed cells on a glass slide.

In the selectivity test also MCF7, a breast cell line down-expressing the α-1 isoform of folic acid receptors, was employed. The cells were maintained in culture in DMEM medium, supplemented with L-glutamine (2 mM), penicillin (100 units/mL), streptomycin (100 μg/mL), and 10% heat-inactivated fetal bovine serum at 37 °C and under 5% CO_2 atmosphere.

In the multiplexing assay, two FA-MFNB samples were prepared by using two different color emitting QDs (green emission, with an emission wavelength of 525 nm, and orange emission, with an emission wavelength of 590 nm). KB cells were doped separately with the two samples. The fixed cells were counted and mixed to obtain an equal ratio of green and orange doped cells. Then, the mixture was drop casted on a glass slide for confocal microscope analysis.

For the cell sorting assay, 5×10^5 cells were doped as described above. After the washing step, the cells were counted and mixed with different ratios (50%, 25%, 10%, 5%, 2.5%, and 1% of doped cells) with control cells. The cell suspension was transferred into a vial, and an NdFeB magnet was placed nearby for 30 min. Finally, the supernatant cells portion and the attracted cells portion were collected and counted.

Preparation of Doped KB Cells for TEM Analysis. KB cells (1.5×10^6) were doped as described above in 1.5 mL of folate-free RPMI-1640 containing 32.5 μg/mL of metal ions. After doping for 1 h, the cells were washed three times in 0.1 M cacodylate buffer and fixed with 2.5% glutaraldehyde in cacodylate buffer at 4 °C for 30 min. The fixed cells were washed three times with cacodylate buffer, and then 1% osmium tetroxide in cacodylate buffer was added for 1 h at room temperature. After another three washing steps in cacodylate buffer, the cells were dehydrated with 30%, 50%, 75%, 85%, 95%, and 100% (three times) absolute ethanol. Thereafter, the cells were infiltrated with Epon resin (two steps: 50% and 66% for resin in absolute ethanol, 30 min each one) and embedded in 100% resin at 60 °C for 48 h. Ultrathin sections (70 nm thick) were cut on an Ultramicrotome (Leika) stained with lead citrate and observed under a JEOL JEM-1011 microscope operating at 100 kV.

Supporting Information Available: Additional experimental details, size distribution graphs, dynamic light scattering, spectroscopic data, and confocal and TEM images of control experiments with cells are available free of charge *via* the Internet at http://pubs.acs.org.

Acknowledgment. This work was supported in part by the European project Magnifyco (Contract NMP4-SL-2009-228622). We thank Mario Malerba for TEM sample preparation and Rosanna Mastria and Angela Fiore for QD sample preparation.

REFERENCES AND NOTES

1. Cozzoli, P. D.; Pellegrino, T.; Manna, L. Synthesis, properties and perspectives of hybrid nanocrystal structures. *Chem. Soc. Rev.* **2006,** *35*, 1195–1208.
2. Talapin, D. V.; Lee, J. S.; Kovalenko, M. V.; Shevchenko, E. V. Prospects of colloidal nanocrystals for electronic and optoelectronic applications. *Chem. Rev.* **2010,** *110*, 389–458.
3. De, M.; Ghosh, P. S.; Rotello, V. M. Applications of nanoparticles in biology. *Adv. Mater.* **2008,** *20*, 4225–4241.
4. Figuerola, A.; Di Corato, R.; Manna, L.; Pellegrino, T. From iron oxide nanoparticles towards advanced iron-based inorganic materials designed for biomedical applications. *Pharmacol. Res.* **2010,** *62*, 126–143.
5. Roca, A. G.; Costo, R.; Rebolledo, A. F.; Veintemillas-Verdaguer, S.; Tartaj, P.; Gonzalez-Carreno, T.; Morales, M. P.; Serna, C. J. Progress in the preparation of magnetic nanoparticles for applications in biomedicine. *J. Phys. D: Appl. Phys.* **2009,** 42.
6. Vats, N.; Wilhelm, C.; Rautou, P. E.; Poirier-Quinot, M.; Pechoux, C.; Devue, C.; Boulanger, C. M.; Gazeau, F. Magnetic tagging of cell-derived microparticles: new prospects for imaging and manipulation of these mediators of biological information. *Nanomedicine* **2010,** *5*, 727–738.
7. Bruns, O. T.; Ittrich, H.; Peldschus, K.; Kaul, M. G.; Tromsdorf, U. I.; Lauterwasser, J.; Nikolic, M. S.; Mollwitz, B.; Merkell, M.; Bigall, N. C..; *et al.* Real-time magnetic resonance imaging and quantification of lipoprotein metabolism *in vivo* using nanocrystals. *Nat. Nanotechnol.* **2009,** *4*, 193–201.
8. Xu, C. J.; Sun, S. H. Monodisperse magnetic nanoparticles for biomedical applications. *Polym. Int.* **2007,** *56*, 821–826.
9. Reiss, P.; Protiere, M.; Li, L. Core/shell semiconductor nanocrystals. *Small* **2009,** *5*, 154–168.
10. Peng, X. G. Band gap and composition engineering on a nanocrystal (BCEN) in solution. *Acc. Chem. Res.* 2010, ASAP.
11. Smith, A. M.; Duan, H. W.; Mohs, A. M.; Nie, S. M. Bioconjugated quantum dots for *in vivo* molecular and cellular imaging. *Adv. Drug Delivery Rev.* **2008,** *60*, 1226–1240.
12. Bruchez, M.; Moronne, M.; Gin, P.; Weiss, S.; Alivisatos, A. P. Semiconductor nanocrystals as fluorescent biological labels. *Science* **1998,** *281*, 2013–2016.

13. Medintz, I. L.; Mattoussi, H.; Clapp, A. R. Potential clinical applications of quantum dots. *Int. J. Nanomed.* **2008,** *3*, 151–167.
14. Lee, J. H.; Huh, Y. M.; Jun, Y. W.; Seo, Y. W.; Jang, J. T.; Song, H. T.; Kim, S.; Cho, E. J.; Yoon, H. G.; S., S. J.; Cheon, J. Artificially engineered magnetic nanoparticles for ultra-sensitive molecular imaging. *Nat. Med.* **2006,** *13*, 95–99; *Nat. Med.* **2006,** *13*, 95–99.
15. Howes, P.; Green, M.; Bowers, A.; Parker, D.; Varma, G.; Kallumadil, M.; Hughes, M.; Warley, A.; Brain, A.; Botnar, R. Magnetic conjugated polymer nanoparticles as bimodal imaging agents. *J. Am. Chem. Soc.* **2010,** *132*, 9833–9842.
16. Corr, S. A.; Rakovich, Y. P.; Gun'ko, Y. K. Multifunctional magnetic-fluorescent nanocomposites for biomedical applications. *Nanoscale Res. Lett.* **2008,** *3*, 87–104.
17. Quarta, A.; Di Corato, R.; Manna, L.; Argentiere, S.; Cingolani, R.; Barbarella, G.; Pellegrino, T. Multifunctional nanostructures based on inorganic nanoparticles and oligothiophenes and their exploitation for cellular studies. *J. Am. Chem. Soc.* **2008,** *130*, 10545–10555.
18. Sun, P.; Zhang, H. Y.; Liu, C.; Fang, J.; Wang, M.; Chen, J.; Zhang, J. P.; Mao, C. B.; Xu, S. K. Preparation and characterization of Fe_3O_4/CdTe magnetic/fluorescent nanocomposites and their applications in immuno-labeling and fluorescent imaging of cancer cells. *Langmuir* **2010,** *26*, 1278–1284.
19. Mi, C. C.; Zhang, J. P.; Gao, H. Y.; Wu, X. L.; Wang, M.; Wu, Y. F.; Di, Y. Q.; Xu, Z. R.; Mao, C. B.; Xu, S. K. Multifunctional nanocomposites of superparamagnetic (Fe_3O_4) and NIR-responsive rare earth-doped up-conversion fluorescent ($NaYF_4$: Yb, Er) nanoparticles and their applications in biolabeling and fluorescent imaging of cancer cells. *Nanoscale* **2010,** *2*, 1141–1148.
20. Lehmann, A. D.; Parak, W. J.; Zhang, F.; Ali, Z.; Rocker, C.; Nienhaus, G. U.; Gehr, P.; Rothen-Rutishauser, B. Fluorescent-magnetic hybrid nanoparticles induce a dose-dependent increase in proinflammatory response in lung cells *in vitro* correlated with intracellular localization. *Small* **2010,** *6*, 753–762.
21. Du, G. H.; Liu, Z. L.; Lu, Q. H.; Xia, X.; Jia, L. H.; Yao, K. L.; Chu, Q.; Zhang, S. M. Fe_3O_4/CdSe/ZnS magnetic fluorescent bifunctional nanocomposites. *Nanotechnology* **2006,** *17*, 2850–2854.
22. Erogbogbo, F.; Yong, K. T.; Hu, R.; Law, W. C.; Ding, H.; Chang, C. W.; Prasad, P. N.; Swihart, M. T. Biocompatible magnetofluorescent probes: luminescent silicon quantum dots coupled with superparamagnetic iron(III) oxide. *ACS Nano* **2010,** *4*, 5131–5138.
23. Chu, M. Q.; Song, X.; Cheng, D.; Liu, S. P.; Zhu, J. Preparation of quantum dot-coated magnetic polystyrene nanospheres for cancer cell labelling and separation. *Nanotechnology* **2006,** *17*, 3268–3273.
24. Corsi, F.; De Palma, C.; Colombo, M.; Allevi, R.; Nebuloni, M.; Ronchi, S.; Rizzi, G.; Tosoni, A.; Trabucchi, E.; Clementi, *et al.* Towards ideal magnetofluorescent nanoparticles for bimodal detection of breast-cancer cells. *Small* **2009,** *5*, 2555–2564.
25. Quarta, A.; Di Corato, R.; Manna, L.; Ragusa, A.; Pellegrino, T. Fluorescent-magnetic hybrid nanostructures: preparation, properties, and applications in biology. *IEEE Trans. Nanobiosci.* **2007,** *6*, 298–308.
26. Insin, N.; Tracy, J. B.; Lee, H.; Zimmer, J. P.; Westervelt, R. M.; Bawendi, M. G. Incorporation of iron oxide nanoplarticles and quantum dots into silica microspheres. *ACS Nano* **2008,** *2*, 197–202.
27. Wang, D. S.; He, J. B.; Rosenzweig, N.; Rosenzweig, Z. Superparamagnetic Fe_2O_3 beads-CdSe/ZnS quantum dots core-shell nanocomposite particles for cell separation. *Nano Lett.* **2004,** *4*, 409–413.
28. LesliePelecky, D. L.; Rieke, R. D. Magnetic properties of nanostructured materials. *Chem. Mater.* **1996,** *8*, 1770–1783.
29. Pileni, M. P. Self-assembly of inorganic magnetic nanocrystals: a new physics emerges. *J. Phys. D: Appl. Phys.* **2008,** 41.
30. Ge, Y. Q.; Zhang, Y.; He, S. Y.; Nie, F.; Teng, G. J.; Gu, N. Fluorescence modified chitosan-coated magnetic nanoparticles for high-efficient cellular imaging. *Nanoscale Res. Lett.* **2009,** *4*, 287–295.
31. Xiao, Q.; Xiao, C. Preparation and characterization of silica-coated magnetic-fluorescent bifunctional microspheres. *Nanoscale Res. Lett.* **2009,** *4*, 1078–1084.
32. Di Corato, R.; Piacenza, P.; Musaro, M.; Buonsanti, R.; Cozzoli, P. D.; Zambianchi, M.; Barbarella, G.; Cingolani, R.; Manna, L.; Pellegrino, T. Magnetic-fluorescent colloidal nanobeads: preparation and exploitation in cell separation experiments. *Macromol. Biosci.* **2009,** *9*, 952–958.
33. Sukhorukov, G. B.; Rogach, A. L.; Garstka, M.; Springer, S.; Parak, W. J.; Munoz-Javier, A.; Kreft, O.; Skirtach, A. G.; Susha, A. S.; Ramaye, Y.; Palankar, R.; Winterhalter, M. Multifunctionalized polymer microcapsules: Novel tools for biological and pharmacological applications. *Small* **2007,** *3*, 944–955.
34. Taboada, E.; Solanas, R.; Rodriguez, E.; Weissleder, R.; Roig, A. Supercritical-fluid-assisted one-pot synthesis of biocompatible core(gamma-Fe_2O_3)/shell(SiO_2) nanoparticles as high relaxivity T-2-contrast agents for magnetic resonance imaging. *Adv. Funct. Mater.* **2009,** *19*, 2319–2324.
35. Sathe, T. R.; Agrawal, A.; Nie, S. M. Mesoporous silica beads embedded with semiconductor quantum dots and iron oxide nanocrystals: Dual-function microcarriers for optical encoding and magnetic separation. *Anal. Chem.* **2006,** *78*, 5627–5632.
36. Resch-Genger, U.; Grabolle, M.; Cavaliere-Jaricot, S.; Nitschke, R.; Nann, T. Quantum dots versus organic dyes as fluorescent labels. *Nat. Methods* **2008,** *5*, 763–775.
37. Yang, J.; Dave, S. R.; Gao, X. H. Quantum dot nanobarcodes: Epitaxial assembly of nanoparticle-polymer complexes in homogeneous solution. *J. Am. Chem. Soc.* **2008,** *130*, 5286–5292.
38. Yang, P.; Murase, N.; Suzuki, M.; Hosokawa, C.; Kawasaki, K.; Kato, T.; Taguchi, T. Bright, non-blinking, and less-cytotoxic SiO_2 beads with multiple CdSe/ZnS nanocrystals. *Chem. Commun.* **2010,** *46*, 4595–4597.
39. Rauf, S.; Glidle, A.; Cooper, J. M. Production of quantum dot barcodes using biological self-assembly. *Adv. Mater.* **2009,** *21*, 4020.
40. Lewinski, N.; Colvin, V.; Drezek, R. Cytotoxicity of nanoparticles. *Small* **2008,** *4*, 26–49.
41. Kirchner, C.; Liedl, T.; Kudera, S.; Pellegrino, T.; Javier, A. M.; Gaub, H. E.; Stolzle, S.; Fertig, N.; Parak, W. J. Cytotoxicity of colloidal CdSe and CdSe/ZnS nanoparticles. *Nano Lett.* **2005,** *5*, 331–338.
42. Rogach, A. L.; Klar, T. A.; Lupton, J. M.; Meijerink, A.; Feldmann, J. Energy transfer with semiconductor nanocrystals. *J. Mater. Chem.* **2009,** *19*, 1208–1221.
43. Lutich, A. A.; Jiang, G.; Susha, A. S.; Rogach, A. L.; Stefani, F. D.; Feldmann, J. Energy transfer versus charge separation in type-II hybrid organic-inorganic nanocomposites. *Nano Lett.* **2009,** *9*, 2636–2640.
44. Stoferle, T.; Scherf, U.; Mahrt, R. F. Energy transfer in hybrid organic/inorganic nanocomposites. *Nano Lett.* **2009,** *9*, 453–456.
45. Sonvico, F.; Mornet, S.; Vasseur, S.; Dubernet, C.; Jaillard, D.; Degrouard, J.; Hoebeke, J.; Duguet, E.; Colombo, P.; Couvreur, P. Folate-conjugated iron oxide nanoparticles for solid tumor targeting as potential specific magnetic hyperthermia mediators: Synthesis, physicochemical characterization, and *in vitro* experiments. *Bioconjugate Chem.* **2005,** *16*, 1181–1188.
46. Mandal, S. K.; Lequeux, N.; Rotenberg, B.; Tramier, M.; Fattaccioli, J.; Bibette, J.; Dubertret, B. Encapsulation of magnetic and fluorescent nanoparticles in emulsion droplets. *Langmuir* **2005,** *21*, 4175–4179.
47. Zebli, B.; Susha, A. S.; Sukhorukov, G. B.; Rogach, A. L.; Parak, W. J. Magnetic targeting and cellular uptake of polymer microcapsules simultaneously functionalized with magnetic and luminescent nanocrystals. *Langmuir* **2005,** *21*, 4262–4265.

48. Adams, J. D.; Kim, U.; Soh, H. T. Multitarget magnetic activated cell sorter. *Proc. Natl. Acad. Sci. U. S. A.* **2008,** *105*, 18165–18170.
49. Wang, G. P.; Song, E. Q.; Xie, H. Y.; Zhang, Z. L.; Tian, Z. Q.; Zuo, C.; Pang, D. W.; Wu, D. C.; Shi, Y. B. Biofunctionalization of fluorescent-magnetic-bifunctional nanospheres and their applications. *Chem. Commun.* **2005,** 4276–4278.
50. Agarwal, M.; Koelling, K. W.; Chalmers, J. J. Characterization of the degradation of polylactic acid polymer in a solid substrate environment. *Biotechnol. Prog.* **1998,** *14*, 517–526.
51. Zeng, H.; Rice, P. M.; Wang, S. X.; Sun, S. H. Shape-controlled synthesis and shape-induced texture of $MnFe_2O_4$ nanoparticles. *J. Am. Chem. Soc.* **2004,** *126*, 11458–11459.
52. Dabbousi, B. O.; RodriguezViejo, J.; Mikulec, F. V.; Heine, J. R.; Mattoussi, H.; Ober, R.; Jensen, K. F.; Bawendi, M. G. (CdSe)ZnS core-shell quantum dots: Synthesis and characterization of a size series of highly luminescent nanocrystallites. *J. Phys. Chem. B* **1997,** *101*, 9463–9475.
53. Yu, W. W.; Qu, L. H.; Guo, W. Z.; Peng, X. G. Experimental determination of the extinction coefficient of CdTe, CdSe, and CdS nanocrystals. *Chem. Mater.* **2003,** *15*, 2854–2860.